Activating the nuclear piston mechanism of 3D migration in tumor cells

Ryan J. Petrie,[1] Heather M. Harlin,[1] Lulu I T. Korsak,[1] and Kenneth M. Yamada[2]

[1]Department of Biology, Drexel University, Philadelphia, PA 19104
[2]Laboratory of Cell and Developmental Biology, National Institute of Dental and Craniofacial Research, National Institutes of Health, Bethesda, MD 20892

Primary human fibroblasts have the remarkable ability to use their nucleus like a piston, switching from low- to high-pressure protrusions in response to the surrounding three-dimensional (3D) matrix. Although migrating tumor cells can also change how they migrate in response to the 3D matrix, it is not clear if they can switch between high- and low-pressure protrusions like primary fibroblasts. We report that unlike primary fibroblasts, the nuclear piston is not active in fibrosarcoma cells. Protease inhibition rescued the nuclear piston mechanism in polarized HT1080 and SW684 cells and generated compartmentalized pressure. Achieving compartmentalized pressure required the nucleoskeleton–cytoskeleton linker protein nesprin 3, actomyosin contractility, and integrin-mediated adhesion, consistent with lobopodia-based fibroblast migration. In addition, this activation of the nuclear piston mechanism slowed the 3D movement of HT1080 cells. Together, these data indicate that inhibiting protease activity during polarized tumor cell 3D migration is sufficient to restore the nuclear piston migration mechanism with compartmentalized pressure characteristic of nonmalignant cells.

Introduction

The movement of single cells through 3D material is essential for normal wound healing, but can become lethal in metastatic disease (Singer and Clark, 1999; Valastyan and Weinberg, 2011). Investigating how cells move through 3D ECM has revealed a multitude of cell migration mechanisms (Friedl and Wolf, 2010; Petrie and Yamada, 2012; Charras and Sahai, 2014). In fact, many cell types can switch between two or more distinct mechanisms, or modes, of movement in response to their environment (Wolf et al., 2003; Petrie et al., 2012; Liu et al., 2015; Madsen et al., 2015; Ruprecht et al., 2015). Deciphering the regulation of this migratory plasticity will be required for comprehensive understanding of both normal and metastatic 3D cell motility.

Adherent primary human fibroblasts switch from using low-pressure lamellipodia to high-pressure lobopodial protrusions when moving through a highly cross-linked 3D matrix, such as those found in mammalian dermis and cell-derived matrix (CDM; Petrie et al., 2012). Additionally, nonadherent fibroblasts can use a third distinct mode of 3D migration, termed A1 amoeboid (Liu et al., 2015). In lobopodial fibroblasts, actomyosin contractility pulls the nucleus forward like a piston in a cylinder to increase cytoplasmic hydraulic pressure in front of the nucleus (Petrie et al., 2014). It is this compartmentalized pressure that drives the lobopodial membrane forward rather than the actin polymerization-mediated brownian ratchet associated with lamellipodial protrusion. This nuclear piston mechanism is used for the efficient movement of primary fibroblasts through cross-linked 3D matrix.

Metastatic cells migrating through 3D matrix can also switch between distinct modes of migration (Sahai and Marshall, 2003; Wolf et al., 2003; Madsen et al., 2015). For example, adherent, elongated (mesenchymal) tumor cells use matrix metalloproteinases (MMPs) to enlarge the pore size of 3D collagen gels to move their bulky nucleus through confined environments (Yu et al., 2012; Wolf et al., 2013; Davidson et al., 2014; Harada et al., 2014; Denais et al., 2016). When protease activity is reduced, these cells increase actomyosin contractility and become round (amoeboid) and less adherent (Wolf et al., 2003; Bergert et al., 2015; Madsen et al., 2015). This increase in actomyosin contractility initiates bleb-based 3D migration and allows the rounded cells to use rapid, adhesion-independent motility to move through the intact 3D matrix (Lämmermann et al., 2008; Liu et al., 2015; Ruprecht et al., 2015). This amoeboid–mesenchymal switch was first identified in HT1080 cells stably expressing MT1-MMP (HT1080/MT1) (Wolf et al., 2003), but it can occur in a variety of cell types (Sanz-Moreno et al., 2008; Ruprecht et al., 2015).

Although it is clear that primary fibroblasts and tumor cells can switch between distinct modes of migration, it is unclear if they switch between the same modes or their migratory plasticity is regulated by similar mechanisms. To test the hypothesis that the migratory plasticity of primary fibroblasts and

Correspondence to Ryan J. Petrie: rjp336@drexel.edu

Abbreviations used: CDM, cell-derived matrix; HFF, human foreskin fibroblast; MLC2, myosin light chain 2; MMP, matrix metalloproteinase.

The Rockefeller University Press $30.00
J. Cell Biol. Vol. 216 No. 1 93–100
https://doi.org/10.1083/jcb.201605097

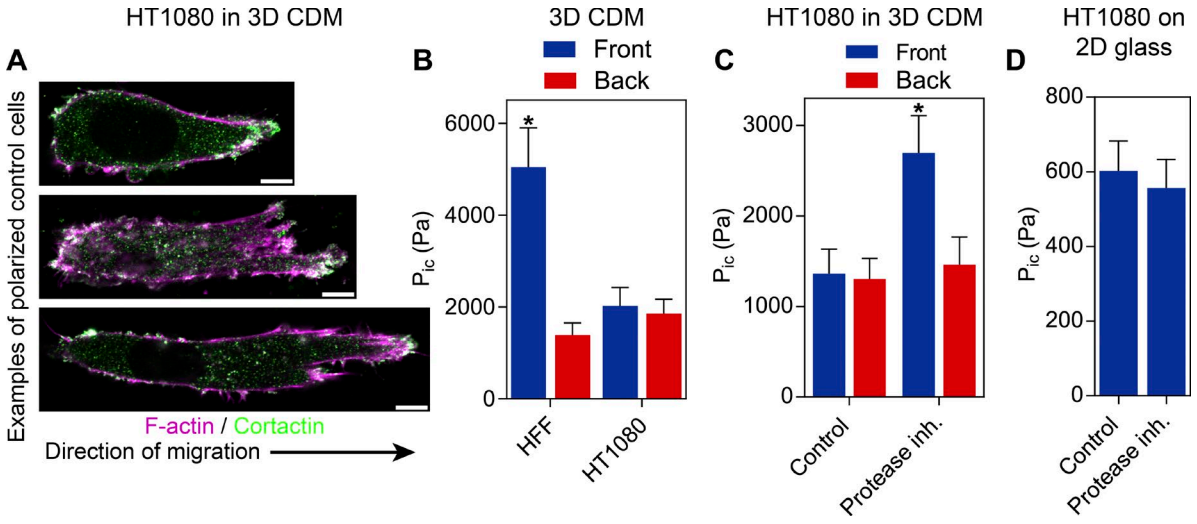

Figure 1. **Protease inhibition selectively increases anterior pressure in fibrosarcoma cells.** (A) The majority of HT1080/MT1 cells migrating in 3D CDM adopt a polarized morphology with a clear leading and trailing edge of varying lengths (n = 45, N = 3). Bars, 10 µm. (B) Polarized HT1080/MT1 cells migrating in 3D CDM have low and uniform intracellular pressure (P_{ic}, measured in Pascals [Pa]) in control cells compared with the compartmentalized pressure in primary human fibroblasts (n = 18, N = 3). (C) Addition of a protease inhibitor (inh.) mixture (Wolf et al., 2003; see Materials and methods) triggers increased intracellular pressure anterior to the nucleus in HT1080/MT1 cells (n = 20, N = 3). (D) HT1080/MT1 cells migrating on 2D glass fail to respond to protease inhibition by raising or compartmentalizing their intracellular pressure (n = 20, N = 3; P = 0.7). Error bars indicate SEM. *, P < 0.01 versus the anterior compartment.

their malignant counterpart differ, we searched for the fibroblast nuclear piston mechanism in polarized HT1080 fibrosarcoma cells moving through 3D CDM. Specifically, we compared the intracellular pressure in front of and behind the nucleus in these cells. We find that the nuclear piston mechanism is normally inactive in fibrosarcoma cells, but it can be activated in elongated, polarized tumor cells by inhibiting MMP activity.

Results and discussion

To establish if single, migrating tumor cells can use the nuclear piston mechanism to generate high-pressure lobopodial protrusions, we first measured the pressure in polarized HT1080/MT1 cells in linearly elastic 3D CDM. Importantly, CDM is the same material that triggers the nuclear piston mechanism in primary fibroblasts, intestinal myofibroblasts, and dedifferentiated chondrocytes (Petrie et al., 2014). In 3D CDM, the majority (76 ± 3%; N = 3) of HT1080/MT1 cells are polarized, with a uniaxial morphology (averaging 54 ± 3 µm in length; n = 45), a rounded trailing edge, and a tapering anterior protrusion (Fig. 1 A). In contrast to primary fibroblasts in the identical ECM (Petrie et al., 2014), intracellular pressure was relatively low and uniform in these cells (Fig. 1 B), indicating that the nuclear piston mechanism was not active.

Because fibroblasts do not use high-pressure lobopodia in protease-treated CDM (Petrie et al., 2012), we hypothesized that cellular protease activity could be modifying local matrix structure to prevent the activation of the nuclear piston mechanism in the HT1080/MT1 cells. To test this hypothesis, we treated HT1080/MT1 cells migrating through 3D CDM with a mixture of protease inhibitors shown to be effective with this cell type (Wolf et al., 2003). Upon protease inhibition, the nuclear piston appeared to become active in polarized cells because there was a significant increase in intracellular pressure in front of the nucleus compared with behind (Fig. 1 C). Despite this increase in pressure, there was no significant decrease in the length of the polarized HT1080/MT1 cells toward an amoeboid phenotype (54 ± 3 vs. 65 ± 4 µm in control and treated cells, respectively; n = 45). In contrast, protease inhibition did not affect the intracellular pressure of these cells moving on 2D glass (Fig. 1 D). We then determined if the pressure generation response was restricted to the HT1080 cells expressing MT1-MMP. We found the broad-spectrum MMP inhibitor GM6001 (Wolf et al., 2013) was sufficient to induce the increase in compartmentalized pressure in control HT1080 cells (HT1080/neo), HT1080 cells obtained directly from American Type Culture Collection (HT1080/ATCC), as well as the human fibrosarcoma cell line SW684 (Fig. S1). Interestingly, control MDA-MB-231 (breast adenocarcinoma) cells generate compartmentalized pressure like primary fibroblasts, whereas the pressure in A549 (lung adenocarcinoma) and SK-MEL-28 (melanoma) cells does not change in response to GM6001. Together, this demonstrates that MMP inhibition is capable of activating the nuclear piston mechanism in multiple fibrosarcoma tumor cell lines, specifically in a 3D matrix.

To confirm that protease inhibition was activating the nuclear piston in HT1080/MT1 cells, we compared the motions of the nucleus and trailing edge within individual cells. In primary fibroblasts using the nuclear piston mechanism, the nucleus moves independently of the trailing edge, consistent with it being pulled forward rather than pushed by myosin II activity (Petrie et al., 2014; Wu et al., 2014). HT1080/MT1 cells were transfected with GFP–myosin light chain 2 (MLC2) and RFP-NLS to highlight the trailing edge and nucleus, respectively (Fig. 2, A and B; and Videos 1 and 2). In control cells moving through 3D CDM, the nucleus and trailing edge tended to move simultaneously. Upon protease inhibition, however, the nucleus and trailing edge moved independently of one another, consistent with the nucleus being pulled forward by the nuclear piston mechanism (Petrie et al., 2014). This was confirmed by plotting the instantaneous velocities of the nucleus and trailing

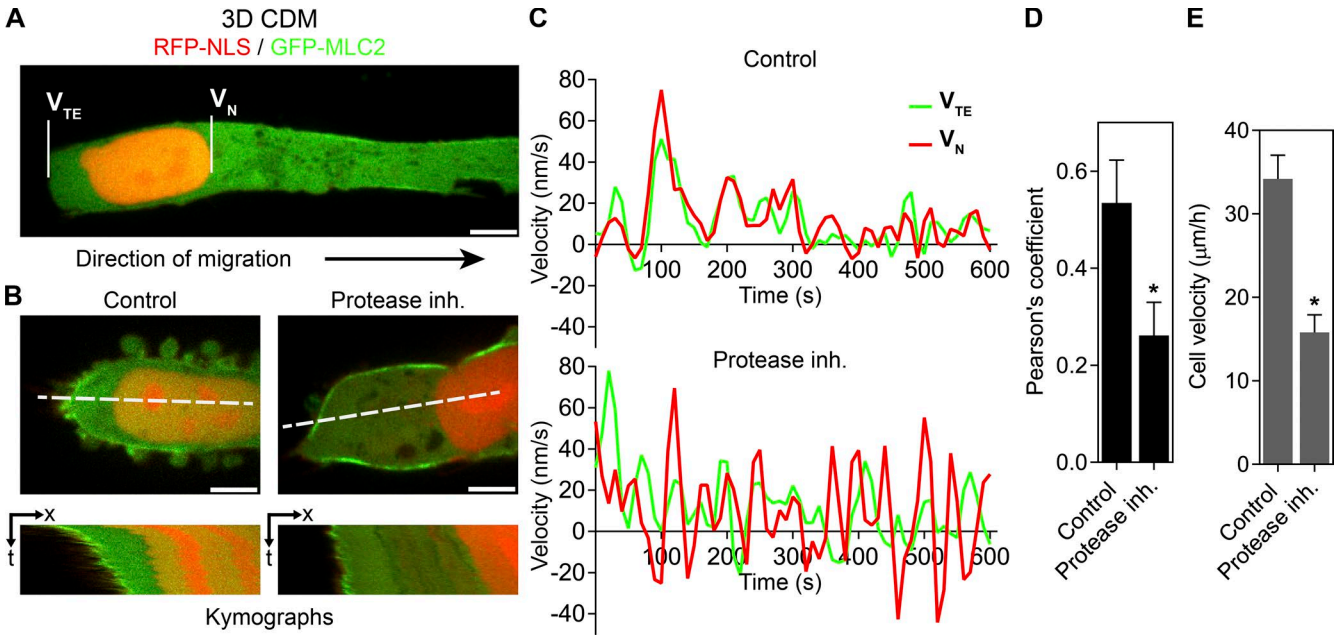

Figure 2. **Protease inhibition activates the nuclear piston and slows cell velocity.** (A) HT1080/MT1 cells were transfected with GFP-MLC2 and RFP-NLS to highlight the trailing edge (TE) and nucleus (N), respectively. Bar, 5 µm. (B) Kymographs of live-cell imaging sequences showing that in control cells, the nucleus (V_N, velocity nucleus) moves synchronously with the trailing edge (V_{TE}, velocity trailing edge; left panels), whereas in protease inhibitor–treated cells, the nucleus can undergo acceleration away from the trailing edge (right panels). Bars, 5 µM. (C) Examples of instantaneous velocity plots of the nucleus (red) versus the trailing edge (green) showing the independent movement of the nucleus in response to protease inhibition (inh.; bottom) compared with a control cell (top). (D) Pearson's correlation coefficients between the velocity of the nucleus and trailing edge (n = 12, N = 3). *, P < 0.05 versus control cells. (E) The velocity of HT1080/MT1 tumor cells is reduced upon protease inhibition and activation of the nuclear piston (n = 45, N = 3). Error bars indicate SEM. *, P < 0.01 versus control cells.

edge and determining the Pearson's correlation coefficient of their motion (Fig. 2, C and D). This quantification established that protease inhibition triggered independent movement of the nucleus relative to the trailing edge, which, together with the compartmentalized pressure data (Fig. 1 C), shows that protease inhibition of HT1080/MT1 cells is sufficient to activate the nuclear piston and trigger high-pressure, polarized fibrosarcoma cell 3D migration. Importantly, HT1080/MT1 velocity through 3D CDM was reduced significantly upon activation of the nuclear piston mechanism by protease inhibition (Fig. 2 E). This reduction in cell velocity suggests that restoring a normal cell migration phenotype in fibrosarcoma cells can change metastatic cell behavior in 3D environments.

To establish whether pressure differences could distinguish mesenchymal (elongated) and amoeboid (rounded) tumor cells, we measured the intracellular pressures of HT1080/ATCC cells in a 3D type I collagen matrix (Fig. 3 A). Interestingly, intracellular pressure was low regardless of cell shape (Fig. 3 B) or measurement location (Fig. S2 A). Upon MMP inhibition, however, pressure specifically increased in the mesenchymal cells, as well as primary fibroblasts (Fig. S2 B). To test if the nuclear piston is an alternative to collagen proteolysis to move the nucleus through a confining 3D matrix, we compared the response of HT1080/ATCC cells to MMP inhibition in low-porosity 1.7 mg/ml rat tail and high-porosity bovine dermal collagen (Fig. 3, C and G; Wolf et al., 2013). MMP inhibition resulted in higher compartmentalized pressure and reduced cell velocity in rat tail collagen (Fig. 3, D and E; and Video 3) and not in bovine collagen (Fig. 3, H and I; and Video 4). Intriguingly, myosin IIB was polarized in ∼50% of control and treated cells in both types of collagen (Fig. 3, F and J; n = 15, N = 3; P = 0.85). Together, these data show the level of intracellular pressure does not distinguish mesenchymal and amoeboid tumor cells, but that protease inhibition increases the pressure in front of the nucleus of mesenchymal cells, consistent with activation of the nuclear piston mechanism. This response in elongated, polarized cells requires a low-porosity 3D matrix and does not occur on 2D glass. These results suggest the nuclear piston is an alternative mechanism to move the bulky nucleus through confining 3D matrices (Wolf et al., 2013; Petrie et al., 2014).

HT1080 cells are known to switch between protease-dependent and -independent migration mechanisms (Wolf et al., 2003). However, protease-independent motility is characterized by relatively low cell-matrix adhesion (Bergert et al., 2015) and elevated actomyosin contractility (Sahai and Marshall, 2003; Madsen et al., 2015) to allow rounded cells to squeeze through 3D ECM (Lämmermann and Sixt, 2009). In contrast, we found that protease inhibition triggered the nuclear piston mechanism in elongated, polarized HT1080 cells to generate high-pressure protrusions. We therefore hypothesized this high-pressure HT1080 phenotype was consistent with adherent, lobopodial fibroblasts (Petrie et al., 2012, 2014), rather than less adherent, round amoeboid cancer cells. To confirm the similarities between the high-pressure polarized HT1080/MT1 cells after protease inhibition and primary fibroblasts, we directly compared their requirements for integrin-mediated cell-matrix adhesion and actomyosin contractility to generate compartmentalized pressure in 3D CDM. Although control lobopodial fibroblasts used the nuclear piston mechanism, moderate inhibition of αVβ3 and β1 integrins abolished compartmentalized pressure without affecting mean cell length (90 ± 4 vs. 96 ± 6 µm in control and treated cells, respectively; n = 45; Fig. 4, A and B). These

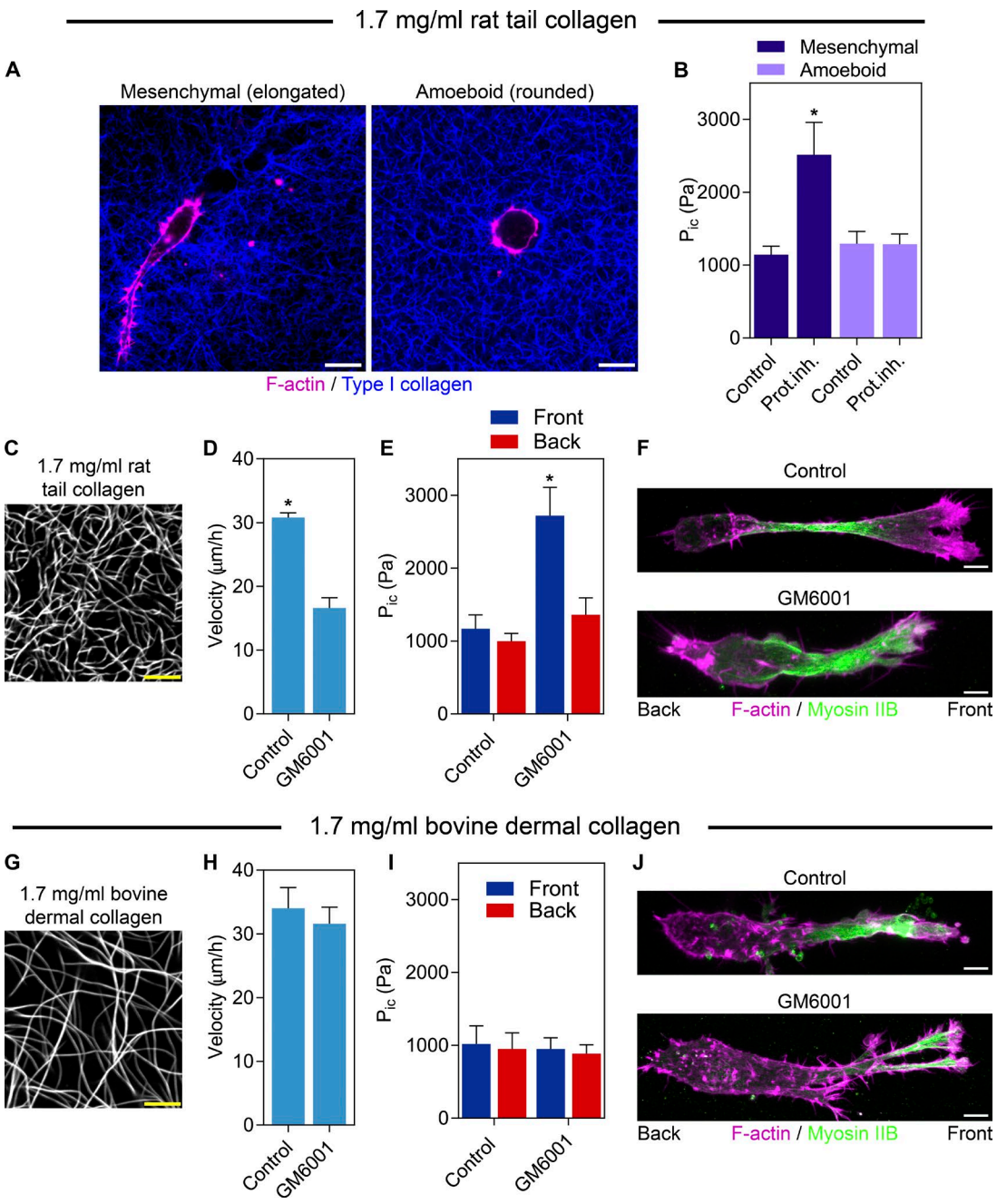

Figure 3. **Protease inhibition increases compartmentalized pressure in mesenchymal tumor cells in low-porosity 3D collagen.** (A) HT1080/ATCC cells in 1.7 mg/ml 3D collagen use either the mesenchymal (elongated) or amoeboid (round) modes of tumor cell migration. Bars, 10 µm. (B) Intracellular pressure (P_{ic}) does not differ significantly between amoeboid and mesenchymal tumor cells moving through 3D collagen. Upon addition of 10 µM GM6001, intracellular pressure specifically increases in mesenchymal tumors cells, whereas the pressure in amoeboid cells does not change (n = 30, N = 3). 1.7 mg/ml rat tail (C) and bovine dermal (G) collagen labeled with Alexa 647. Bars, 5 µM. MMP inhibition significantly slows the velocity (n = 45, N = 3; D) and increases compartmentalized pressure (n = 15, N = 3; E) of HT1080/ATCC cells moving in rat tail collagen, but not bovine dermal collagen (H and I). Myosin IIB localization is unaffected by GM6001 treatment in 1.7 mg/ml rat tail (F) and bovine dermal (J) collagen (n = 15, N = 3). Bars, 10 µM. Error bars indicate SEM. *, P < 0.01 versus control cells.

data indicate the nuclear piston mechanism is integrin dependent. The generation of compartmentalized pressure in HT1080/MT1 cells in response to GM6001 treatment (Fig. 4 E) required integrin-mediated adhesion and actomyosin contractility, similar to the nuclear piston mechanism in lobopodial fibroblasts (Petrie et al., 2014; Fig. 4 B). The velocity of HT1080/MT1 cells was significantly reduced by these treatments compared with control cells (Fig. 4 C). Interestingly, protease inhibition can trigger significant differences in the 3D migration mechanisms used by HT1080/MT1 cells without disrupting cell morphology (Fig. 4 D). Further, the compartmentalized pressure response required nesprin 3, vimentin, and lamin A (Fig. 4, F and G; and Fig. S3). Together, these data indicate that when protease activity is inhibited, polarized HT1080 cells require nesprin 3, actomyosin contractility, and integrin-mediated adhesion generate compartmentalized pressure, similar to lobopodial fibroblasts

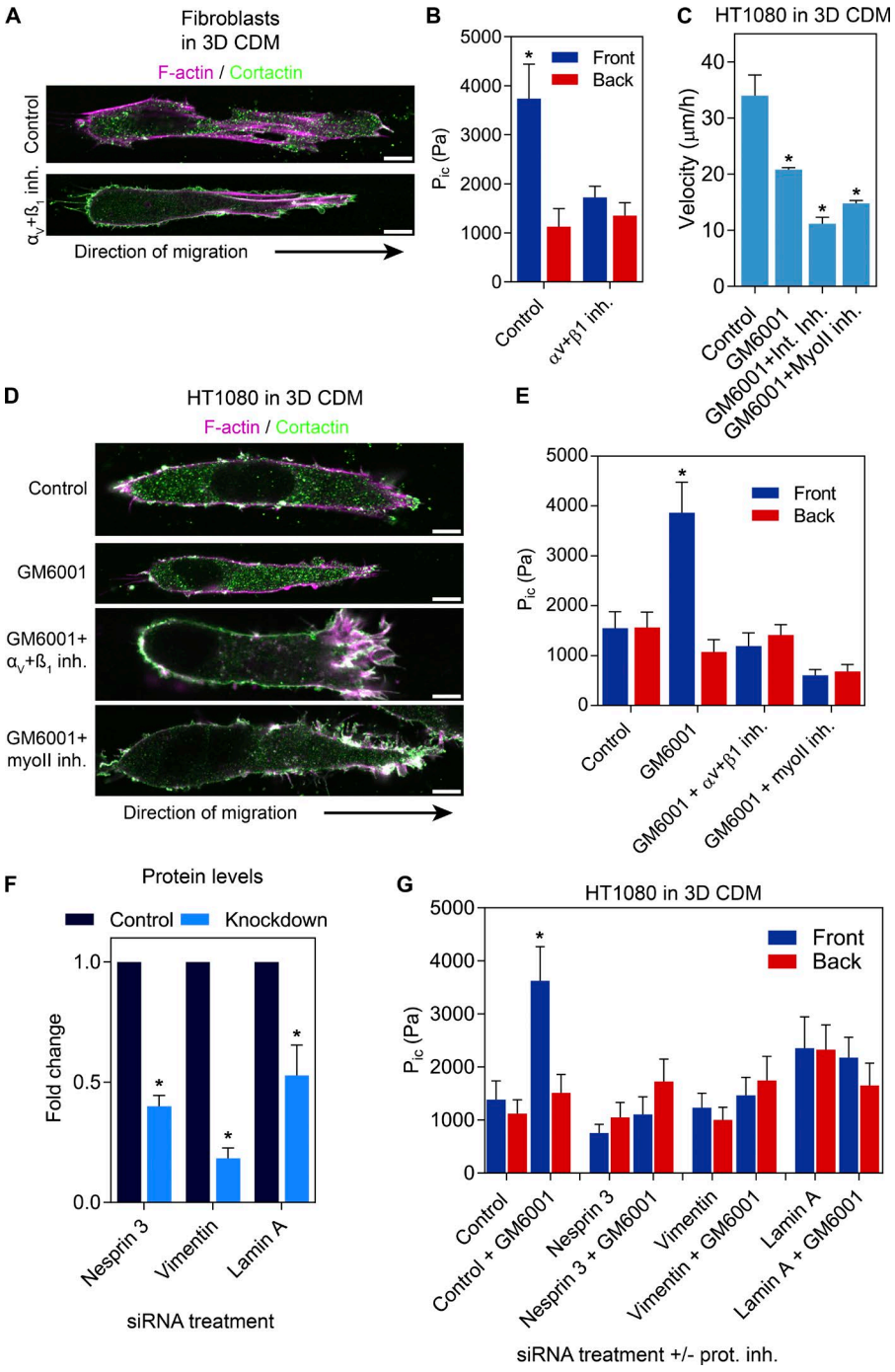

Figure 4. **The nuclear piston mechanism requires integrin-mediated, cell-matrix adhesion, actomyosin contractility, vimentin, nesprin 3, and lamin A.** (A and B) Primary human dermal fibroblasts migrating in 3D CDM use the nuclear piston and compartmentalized pressure. Inhibition of β1 and αV integrins is sufficient to revert the intracellular pressure (P_{ic}) to low and uniform, without completely disrupting cell adhesion (n = 16, N = 3). *, P < 0.001 versus control cells. Bars, 10 µm. (C) The velocity of HT/MT1 cells migrating in 3D CDM either untreated or treated with GM6001, integrin inhibitors (Int. Inh.), or blebbistatin in combination with GM6001 (n = 45, N = 3). *, P < 0.001 versus control cells. (D) Cell morphology of the HT/MT1 cells treated as indicated. Cells can remain polarized with clear leading and trailing edges. Bars, 10 µm. (E) The increased compartmentalized pressure generated by protease inhibition is consistent with the nuclear piston mechanism in lobopodial primary human fibroblasts in that it requires β1 and αV integrins in combination with actomyosin contractility (n = 18, N = 3). *, P < 0.001 versus the anterior compartment. (F) Quantification of the blots represented in Fig. S3 A demonstrating the specificity of siRNA-mediated knockdown of nesprin 3, vimentin, or lamin A using a pool of siRNA sequences (N = 3). *, P < 0.01 versus the control. (G) MMP inhibition does not increase compartmentalized pressure in HT1080 cells in 3D CDM after nesprin 3, vimentin, or lamin A siRNA-mediated protein knockdown (n = 15, N = 3). *, P < 0.001 versus the anterior compartment. Error bars indicate SEM. MyoII inh., myosin II inhibitor.

(Petrie et al., 2014), as well as the intermediate filament proteins vimentin and lamin A.

The generation of compartmentalized pressure in HT1080/MT1 cells in response to GM6001 treatment suggested increased MMP activity could explain the reduced intracellular pressure in fibrosarcoma cells relative to primary human fibroblasts in 3D CDM. Therefore, we overexpressed GFP-tagged MT1-MMP (3.6 ± 1.4-fold vs. endogenous MT1-MMP; n = 15, N = 3; Fig. 5 B) in primary dermal fibroblasts and measured their intracellular pressure to determine if the nuclear piston mechanism was disrupted. GFP-MT1MMP was localized to intracellular vesicles and the plasma membrane, as expected (Marchesin et al., 2015), and did not affect overall cell morphology (Fig. 5 A and Video 5). We measured the pressure in these cells and found that anterior pressure was high in the GFP control, as expected (Fig. 5 C; Petrie et al., 2014). In striking contrast, primary dermal fibroblasts expressing GFP-MT1MMP had relatively low intracellular pressure in front of the nucleus, similar to HT1080/MT1 cells (Fig. 1 B). Importantly, adding the MMP inhibitor GM6001 resulted in the rescue of compartmentalized pressure in fibroblasts expressing GFP-MT1MMP (Fig. 5 C), without affecting cell velocity (Fig. 5 D). Together, these data confirm that inhibition of MMP activity is sufficient to restore nuclear piston function in primary human fibroblasts in 3D CDM expressing GFP-MT1MMP.

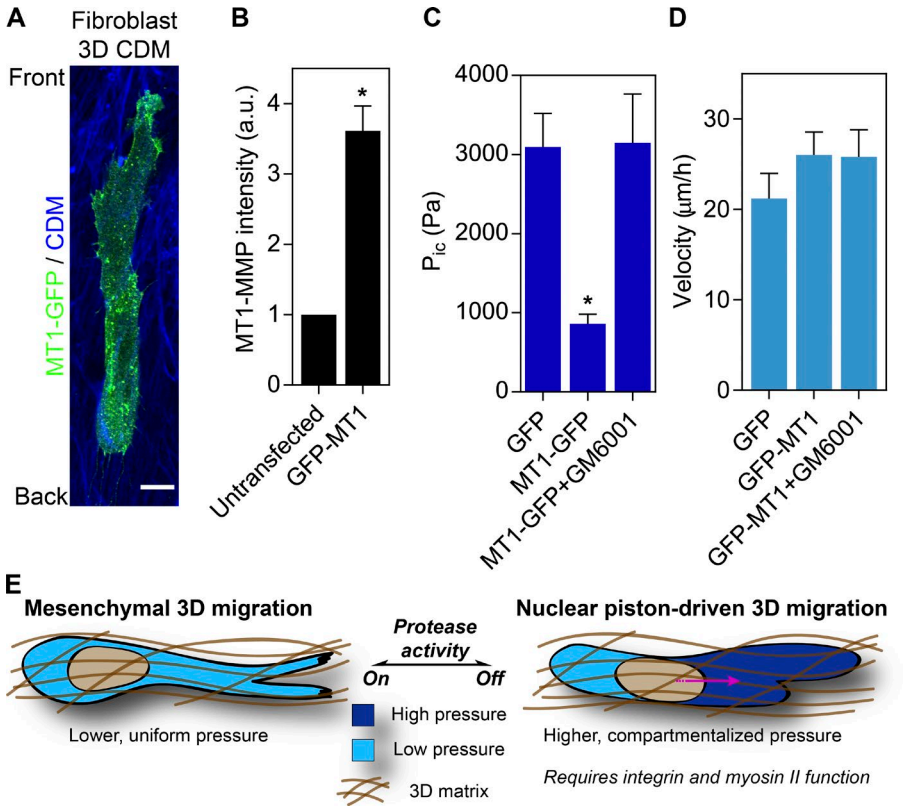

Figure 5. **Exogenous MT1-MMP expression abolishes compartmentalized pressure in primary human fibroblasts.** (A) Morphology of primary human dermal fibroblasts expressing GFP-MT1MMP. GFP-MT1MMP is cytoplasmic in intracellular vesicles and at the plasma membrane (Video 5). Bar, 10 µm. (B) The expression of total MT1MMP in HT1080 cells transiently transfected with GFP-MT1MMP relative to untransfected cells (n = 15, N = 3). *, P < 0.0001 versus untransfected cells. (C) The anterior cytoplasmic intracellular pressure (P_{ic}) in primary human dermal fibroblasts, either transfected with GFP or GFP-MT1MMP and untreated, or transfected with GFP-MT1MMP and treated with 10 µM GM6001 (n = 15, N = 3). *, P < 0.001 versus GFP. (D) The velocity of HT1080 cells transfected with either GFP or GFP-MT1MMP ± GM6001 treatment moving through CDM (n = 30, N = 3). P = 0.44. Error bars indicate SEM. (E) Model. Our data suggest mesenchymal tumor cells use MMP activity to enlarge constricting pores and move the nucleus through the fibrillar 3D matrix without activating the nuclear piston mechanism. When MMP activity is low, either in tumor cells or primary human fibroblasts migrating through 3D ECM, cells rely on robust cell-matrix adhesions and actomyosin contractility to pull the nucleus forward and increase pressure in the anterior cytoplasmic compartment. This nuclear piston mechanism may represent an alternative strategy to move the rigid nucleus through a confining 3D matrix. a.u., arbitrary units.

Conclusions

Unlike primary dermal fibroblasts, polarized fibrosarcoma cells move through 3D CDM using low-pressure protrusions under control conditions. They are, however, capable of switching to high-pressure protrusions upon inhibition of MMP activity. The suppression of the nuclear piston mechanism by elevated MMP activity predicts an increase in proteolytic activity in HT1080 cells relative to primary fibroblasts. In fact, such a difference has been documented previously (Jones and DeClerck, 1980). We speculate that the proteolytic degradation of the 3D ECM and the nuclear piston mechanism represent two distinct, alternative strategies to help move the stiff, bulky nucleus through fibrillar matrix environments (Fig. 5 E; Wolf et al., 2013; Davidson et al., 2014; Harada et al., 2014). Finally, these results demonstrate there can be clear differences between the 3D migration mechanisms of normal primary fibroblasts and their abnormal, transformed fibrosarcoma cell counterparts. Strategies to correct such potential defects in the physical mechanisms of metastatic cell motility may slow their movement through 3D matrices in vitro and in vivo (Surcel et al., 2015).

Materials and methods

Reagents, inhibitor treatments, and cell culture

The reagents used in this study are as follows: rhodamine-phalloidin (Thermo Fisher Scientific), succinimidyl Alexa 647 (Thermo Fisher Scientific), blebbistatin (EMD Millipore), BB-2516 (Sigma-Aldrich), E-64 (Sigma-Aldrich), pepstatin A (Sigma-Aldrich), leupeptin (Sigma-Aldrich, aprotinin (Sigma-Aldrich), GM6001 (EMD Millipore), $\alpha_v\beta_3$- blocking cyclic RGD peptide (Sigma-Aldrich), and β_1-blocking antibody mAb13 (Akiyama et al., 1989). The protease inhibitor mixture consisted of: 100 µM BB-2516, 250 µM E-64, 5 µM pepstatin A, 2 µM leupeptin, and 2.2 µM aprotinin as previously described (Wolf et al., 2003). Cyclic RGD peptide and mAb13 were used at 50 µM and 50 µg/ml, respectively. GM6001 was used at 10 µM, and blebbistatin was used at 25 µM. Cells were treated with the indicated inhibitors for 30 min at 37°C before the pressure measurements or the cell motility studies being performed in the presence of the inhibitor.

Primary human foreskin fibroblasts (HFFs) were used at passages 6–20. HT1080/MT1 and HT1080/neo cell lines were generously provided by P. Friedl (Radboud University Nijmegen Medical Centre, Nijmegen, Netherlands; Wolf et al., 2003). The HT1080/ATCC, SW684, and A549 cells lines were obtained directly from the ATCC. The MDA-MB-231 and SK-MEL-28 cell lines were graciously provided by E. Sahai (The Francis Crick Institute, London, England, UK). All cells were maintained in phenol red–free DME (HyClone Laboratories, Inc.) containing 10% FBS (HyClone Laboratories, Inc.), 4.5 g/liter glucose, 100 U/ml penicillin, 100 µg/ml streptomycin (Invitrogen), and 2 mM L-glutamine (Invitrogen) at 37°C and in 10% CO_2. 3D collagen gels (1.7 mg/ml) and CDM were prepared as described (Petrie et al., 2012). Specifically, 1.7 mg/ml collagen was prepared by adding 10× DME (Invitrogen) and 10× reconstitution buffer (0.2 M Hepes and 0.26 M $NaHCO_3$) to 4.73 mg/ml rat tail type I collagen (Corning) or 3.2 mg/ml bovine dermal collagen (Advanced BioMatrix) at a 1:1:8 ratio. The pH was adjusted to 7.5, and the collagen mixture was diluted to a final concentration of 1.7 mg/ml with medium. To generate CDM, primary human dermal fibroblasts were plated at high density on gelatin-coated and glutaraldehyde-treated 35-mm (4 × 10^5 cells; MatTek Corporation) or 50-mm (5.7 × 10^5 cells; Warner Instruments) glass-bottom dishes. Cell cultures were grown for 10 d, adding fresh media with 50 µg/ml ascorbic acid every second day. The cells were removed from the matrices by the addition of extraction buffer (20 mM NH_4OH and 0.5% Triton X-100 in PBS) for 10 min at RT and washed with PBS.

siRNAs, cDNA constructs, and transfection

Knockdowns were performed using independent siRNAs: nesprin 3 (5′-GCAUCGUCGACGCGCAAAU-3′, 5′-UGGCAGAAUUCCCGG AGAA-3′, 5′-AGGCAGGUGUGGACGAGUU-3′, and 5′-UGAAGG AGCUCAUCGUCUU-3′), vimentin (5′-UCACGAUGACCUUGA AUAA-3′, 5′-GAGGGAAACUAAUCUGGAU-3′, 5′-UUAAGACGG UUGAAACUAG-3′, and 5′-GGAAAUGGCUCGUCACCUU-3′), and lamin A (5′-GAAGGAGGGUGACCUGAUA-3′, 5′-UCACAGCAC GCACGCACUA-3′, 5′-UGAAAGCGCGCAAUACCAA-3′, and 5′-CGUGUGCGCUCGCUGGAAA-3′). ON-TARGETplus SMARTpool siRNAs, along with a Non-targeting siRNA control pool, were purchased from GE Healthcare. The specificities of the siRNA pools were confirmed using the following independent siRNAs (QIAGEN): FlexiTube nesprin 3 (5′-CGCUCAUGCUGCGCUACAATT-3′), vimentin (5′-GGCACGUCUUGACCUUGAATT-3′), and lamin A (5′-GGC AGUCUGCUGAGAGGAATT-3′). HFFs (2×10^5) were transfected with a 20-nM solution of the indicated siRNA preparation using Lipofectamine 2000 (Thermo Fisher Scientific) according to the manufacturer's instructions. After 24 h, 5×10^4 siRNA-treated cells were replated on 3D CDM for pressure measurements the next day.

RFP-NLS and GFP-MLC2 were described previously (Petrie et al., 2014). GFP-MT1MMP was described previously (Liu et al., 2000). All cDNAs were transfected into cells using Lipofectamine 3000 (Thermo Fisher Scientific) according to the manufacturer's instructions.

Western blotting

48 h after transfection with siRNA, HT1080s were lysed in RIPA buffer (1% Triton X-100, 0.5% sodium deoxycholate, 0.1% sodium dodecylsulfate, 150 mM NaCl, and 50 mM Tris, pH 8) plus 1× protease inhibitors without EDTA (Roche). Cleared lysates were combined with an equal volume of 2× sample buffer, heated to 95°C for 5 min, resolved by SDS-PAGE on a 4–12% Tris-glycine polyacrylamide gel (Thermo Fisher Scientific), and transferred to nitrocellulose (0.2-µm pores; Thermo Fisher Scientific). Secondary antibodies used for Western blotting were: goat anti–rabbit IgG Alexa 680 and goat anti–mouse IgG Alexa 680 (Thermo Fisher Scientific). Blots were visualized on an Odyssey Scanner (LI-COR Biosciences). Western blots were quantified by normalizing the signal intensity of nesprin 3, vimentin, or lamin A to the corresponding GAPDH signal and determining the change in expression of the siRNA-mediated protein knockdown relative to the control.

Intracellular pressure measurements

The 900A micropressure system (World Precision Instruments) was used to make direct measurements of intracellular pressure according to the manufacturer's instructions and as described in Petrie and Koo (2014). A 0.5-µm micropipette (World Precision Instruments) was filled with a 1-M KCl solution, placed in a microelectrode holder half-cell (World Precision Instruments), and connected to a pressure source regulated by the 900A system. A calibration chamber (World Precision Instruments) was filled with 0.1 M KCl and connected to the 900A system, and the resistance of each microelectrode was set to zero and then secured in a MPC-325 micromanipulator (Sutter Instrument) within an environmental chamber (37°C and 10% CO_2) on an Axiovert 200M microscope (ZEISS). To measure intracellular pressure, the microelectrode was driven at a 45° angle into the cytoplasm, maintained in place for ≥5 s, and removed. The pressure measurement was calculated as the mean pressure reading during this interval of time. In individual polarized, elongated cells, a pressure measurement was first made behind the nucleus, followed by a measurement in front of the nucleus in the same cell.

Antibodies and immunofluorescence imaging

The following antibodies and reagents were used: rabbit anti–nesprin 3 (provided by D. Starr, University of California, Davis, Davis, CA); mouse anti–cortactin (EMD Millipore), mouse anti–GAPDH (Fitzgerald), mouse anti–vimentin (EMD Millipore), mouse anti–lamin A (EMD Millipore), mouse anti–MT1MMP (EMD Millipore), rabbit anti–myosin IIB (Covance), goat anti–mouse IgG Alexa 488 (Thermo Fisher Scientific), and goat anti–rabbit IgG Alexa 546 (Thermo Fisher Scientific). Cells were fixed with 4% formaldehyde in PBS, permeabilized with 0.25% Triton X-100 in PBS, and blocked with 0.2% BSA in PBS. Rhodamine-phalloidin and primary and secondary antibodies were added in 0.2% BSA in PBS and washed with PBS. A protocol published previously was used to localize myosin IIB in HT1080 cells (Petrie et al., 2014). HT1080 cells embedded in 3D collagen were fixed with 4% formaldehyde and 0.2% glutaraldehyde in PBS for 15 min at RT, washed with 50 mM NH_4Cl in PBS, and chilled for 2 min on ice, with all subsequent steps performed with prechilled solutions on ice. Cells were treated with buffer A (1% BSA, 50 mM NH_4Cl, 0.5% saponin, and 0.005% Triton X-100 in PBS) for 45 min. Primary antibody was added in buffer B (1% BSA, 50 mM NH_4Cl, and 0.1% saponin in PBS) for 1 h. Cells were washed twice with buffer C (1% BSA, 50 mM NH_4Cl, and 0.5% saponin in PBS). Secondary antibody was applied in buffer B for 45 min. Cells were washed twice with buffer C and postfixed with 2% formaldehyde in PBS for 10 min on ice and then 5 min at RT. Cells were washed twice in 50 mM NH_4Cl in PBS and once in PBS before imaging. Cells were imaged using a scanning confocal microscope (510 NLO META Axiovert 200M; ZEISS) with a Plan Apochromat 63×, 1.4 NA oil objective. Brightness and contrast were linearly adjusted using ImageJ 1.47v (National Institutes of Health). An HT1080 cell was classified as amoeboid when its length was less than twice its width (Sanz-Moreno et al., 2008), and the trailing and leading edges could not be distinguished from one another based on phase imaging.

Live-cell fluorescence imaging

HFFs were transfected with RFP-NLS and GFP-MLC2 to visualize the nucleus and trailing edge, respectively, and imaged by spinning-disc confocal microscopy. Specifically, using an Axiovert 200M microscope (ZEISS) equipped with a confocal scanning unit (CSU-X1; Yokogawa Electric Corporation), a Plan Apochromat 63×, 1.4 NA oil objective (ZEISS), and an EM charge-coupled device camera (C9100; Hamamatsu Photonics). Hardware control, image acquisition, and linear brightness and contrast adjustments were performed using MetaMorph software (Molecular Devices). RFP-NLS and GFP-MLC2 were excited with 561- and 488-nm laser light, respectively. Images of live cotransfected cells were acquired every 10 s for 10 min. The JFilament plugin (Smith et al., 2010) was used with ImageJ to measure the instantaneous velocities of the trailing edge and nucleus at each time point as described (Petrie et al., 2014). The measured velocities were plotted, and Pearson's correlation coefficient was calculated with Prism 6 (GraphPad Software).

Motility assays

10^4 HFFs were seeded in 10% FBS in DME onto CDM. The following day, time-lapse movies were captured at 10% CO_2 and 37°C using a 10×, 0.12 NA A-Plan objective on an Axiovert 40C microscope (ZEISS) with a charge-coupled device camera (INFINITY2; Lumenera). Cells were tracked every 26 min for 12 h using the Manual Tracking plugin (F. Cordelieres, Institut Curie, Paris, France) with ImageJ 1.47v. Velocity was calculated from the tracking data using the ImageJ Chemotaxis and Migration Tool plugin (Ibidi).

Statistics

Results are presented as the mean ± SEM, with *n* indicating the total number of data points and *N* indicating the total number of experiments for each condition or cell type. One-way analysis of variance with Tukey posttests were used to compare three or more variables. The

unpaired, two-tailed Student's *t* test was used to compare two variables. All comparisons were performed with Prism 6 (GraphPad Software). Differences were considered statistically significant at $P < 0.05$.

Online supplemental material

Fig. S1 shows the response of intracellular pressure to MMP inhibition in six additional cell lines. Fig. S2 confirms the low pressure of amoeboid HT1080 cells and the activation of the nuclear piston by MMP inhibition in primary human fibroblasts in 3D collagen. Fig. S3 shows examples of Western blots of cells treated with either SMARTpool siRNAs or an independent single siRNA, quantification of the protein knockdown by the independent single siRNAs, as well as their effect on compartmentalized pressure in HT1080 cells. Videos 1 and 2 show the movement of the nucleus and trailing edge in control HT1080 and GM6001-treated HT1080 cells, respectively. Videos 3 and 4 show the effect of MMP inhibition on HT1080 movement in 1.7 mg/ml rat tail and bovine dermal collagen, respectively. Video 5 demonstrates the localization and dynamics of GFP-MT1MMP in primary fibroblasts.

Acknowledgments

The authors thank L. Dolat for suggestions on the manuscript and P. Friedl for generously providing the HT1080 cells.

Work in K.M. Yamada's laboratory is supported by the Intramural Research Program of the National Institutes of Health, National Institute of Dental and Craniofacial Research. R.J. Petrie is supported by startup funds from the College of Arts and Sciences and the Department of Biology of Drexel University.

The authors declare no competing financial interests.

Author contributions: R.J. Petrie designed, performed, and analyzed all of the experiments except for the imaging of HT1080 cells in 3D collagen (performed by H.M. Harlin) and the siRNA experiments and quantification of protein knockdown (performed by H.M. Harlin and L.I.T. Korsak). R.J. Petrie wrote the paper with K.M. Yamada providing essential editorial oversight and critical review.

Submitted: 25 May 2016
Revised: 10 October 2016
Accepted: 2 December 2016

References

Akiyama, S.K., S.S. Yamada, W.T. Chen, and K.M. Yamada. 1989. Analysis of fibronectin receptor function with monoclonal antibodies: Roles in cell adhesion, migration, matrix assembly, and cytoskeletal organization. *J. Cell Biol.* 109:863–875. http://dx.doi.org/10.1083/jcb.109.2.863

Bergert, M., A. Erzberger, R.A. Desai, I.M. Aspalter, A.C. Oates, G. Charras, G. Salbreux, and E.K. Paluch. 2015. Force transmission during adhesion-independent migration. *Nat. Cell Biol.* 17:524–529. http://dx.doi.org/10.1038/ncb3134

Charras, G., and E. Sahai. 2014. Physical influences of the extracellular environment on cell migration. *Nat. Rev. Mol. Cell Biol.* 15:813–824. http://dx.doi.org/10.1038/nrm3897

Davidson, P.M., C. Denais, M.C. Bakshi, and J. Lammerding. 2014. Nuclear deformability constitutes a rate-limiting step during cell migration in 3-D environments. *Cell. Mol. Bioeng.* 7:293–306. http://dx.doi.org/10.1007/s12195-014-0342-y

Denais, C.M., R.M. Gilbert, P. Isermann, A.L. McGregor, M. te Lindert, B. Weigelin, P.M. Davidson, P. Friedl, K. Wolf, and J. Lammerding. 2016. Nuclear envelope rupture and repair during cancer cell migration. *Science.* 352:353–358. http://dx.doi.org/10.1126/science.aad7297

Friedl, P., and K. Wolf. 2010. Plasticity of cell migration: A multiscale tuning model. *J. Cell Biol.* 188:11–19. http://dx.doi.org/10.1083/jcb.200909003

Harada, T., J. Swift, J. Irianto, J.W. Shin, K.R. Spinler, A. Athirasala, R. Diegmiller, P.C. Dingal, I.L. Ivanovska, and D.E. Discher. 2014. Nuclear lamin stiffness is a barrier to 3D migration, but softness can limit survival. *J. Cell Biol.* 204:669–682. http://dx.doi.org/10.1083/jcb.201308029

Jones, P.A., and Y.A. DeClerck. 1980. Destruction of extracellular matrices containing glycoproteins, elastin, and collagen by metastatic human tumor cells. *Cancer Res.* 40:3222–3227.

Lämmermann, T., and M. Sixt. 2009. Mechanical modes of 'amoeboid' cell migration. *Curr. Opin. Cell Biol.* 21:636–644. http://dx.doi.org/10.1016/j.ceb.2009.05.003

Lämmermann, T., B.L. Bader, S.J. Monkley, T. Worbs, R. Wedlich-Soldner, K. Hirsch, M. Keller, R. Forster, D.R. Critchley, R. Fassler, and M. Sixt. 2008. Rapid leukocyte migration by integrin-independent flowing and squeezing. *Nature.* 453:51–55. http://dx.doi.org/10.1038/nature06887

Liu, S., S. Netzel-Arnett, H. Birkedal-Hansen, and S.H. Leppla. 2000. Tumor cell-selective cytotoxicity of matrix metalloproteinase-activated anthrax toxin. *Cancer Res.* 60:6061–6067.

Liu, Y.J., M. Le Berre, F. Lautenschlaeger, P. Maiuri, A. Callan-Jones, M. Heuze, T. Takaki, R. Voituriez, and M. Piel. 2015. Confinement and low adhesion induce fast amoeboid migration of slow mesenchymal cells. *Cell.* 160:659–672. http://dx.doi.org/10.1016/j.cell.2015.01.007

Madsen, C.D., S. Hooper, M. Tozluoglu, A. Bruckbauer, G. Fletcher, J.T. Erler, P.A. Bates, B. Thompson, and E. Sahai. 2015. STRIPAK components determine mode of cancer cell migration and metastasis. *Nat. Cell Biol.* 17:68–80. http://dx.doi.org/10.1038/ncb3083

Marchesin, V., A. Castro-Castro, C. Lodillinsky, A. Castagnino, J. Cyrta, H. Bonsang-Kitzis, L. Fuhrmann, M. Irondelle, E. Infante, G. Montagnac, et al. 2015. ARF6-JIP3/4 regulate endosomal tubules for MT1-MMP exocytosis in cancer invasion. *J. Cell Biol.* 211:339–358. http://dx.doi.org/10.1083/jcb.201506002

Petrie, R.J., and H. Koo. 2014. Direct measurement of intracellular pressure. *Curr. Protoc. Cell Biol.* 63:12.9.1–12.9.9.

Petrie, R.J., and K.M. Yamada. 2012. At the leading edge of three-dimensional cell migration. *J. Cell Sci.* 125:5917–5926. http://dx.doi.org/10.1242/jcs.093732

Petrie, R.J., N. Gavara, R.S. Chadwick, and K.M. Yamada. 2012. Nonpolarized signaling reveals two distinct modes of 3D cell migration. *J. Cell Biol.* 197:439–455. http://dx.doi.org/10.1083/jcb.201201124

Petrie, R.J., H. Koo, and K.M. Yamada. 2014. Generation of compartmentalized pressure by a nuclear piston governs cell motility in a 3D matrix. *Science.* 345:1062–1065. http://dx.doi.org/10.1126/science.1256965

Ruprecht, V., S. Wieser, A. Callan-Jones, M. Smutny, H. Morita, K. Sako, V. Barone, M. Ritsch-Marte, M. Sixt, R. Voituriez, and C.P. Heisenberg. 2015. Cortical contractility triggers a stochastic switch to fast amoeboid cell motility. *Cell.* 160:673–685. http://dx.doi.org/10.1016/j.cell.2015.01.008

Sahai, E., and C.J. Marshall. 2003. Differing modes of tumour cell invasion have distinct requirements for Rho/ROCK signalling and extracellular proteolysis. *Nat. Cell Biol.* 5:711–719. http://dx.doi.org/10.1038/ncb1019

Sanz-Moreno, V., G. Gadea, J. Ahn, H. Paterson, P. Marra, S. Pinner, E. Sahai, and C.J. Marshall. 2008. Rac activation and inactivation control plasticity of tumor cell movement. *Cell.* 135:510–523. http://dx.doi.org/10.1016/j.cell.2008.09.043

Singer, A.J., and R.A. Clark. 1999. Cutaneous wound healing. *N. Engl. J. Med.* 341:738–746. http://dx.doi.org/10.1056/NEJM199909023411006

Smith, M.B., H. Li, T. Shen, X. Huang, E. Yusuf, and D. Vavylonis. 2010. Segmentation and tracking of cytoskeletal filaments using open active contours. *Cytoskeleton.* 67:693–705. http://dx.doi.org/10.1002/cm.20481

Surcel, A., W.P. Ng, H. West-Foyle, Q. Zhu, Y. Ren, L.B. Avery, A.K. Krenc, D.J. Meyers, R.S. Rock, R.A. Anders, et al. 2015. Pharmacological activation of myosin II paralogs to correct cell mechanics defects. *Proc. Natl. Acad. Sci. USA.* 112:1428–1433. http://dx.doi.org/10.1073/pnas.1412592112

Valastyan, S., and R.A. Weinberg. 2011. Tumor metastasis: Molecular insights and evolving paradigms. *Cell.* 147:275–292. http://dx.doi.org/10.1016/j.cell.2011.09.024

Wolf, K., I. Mazo, H. Leung, K. Engelke, U.H. von Andrian, E.I. Deryugina, A.Y. Strongin, E.B. Brocker, and P. Friedl. 2003. Compensation mechanism in tumor cell migration: Mesenchymal-amoeboid transition after blocking of pericellular proteolysis. *J. Cell Biol.* 160:267–277. http://dx.doi.org/10.1083/jcb.200209006

Wolf, K., M. Te Lindert, M. Krause, S. Alexander, J. Te Riet, A.L. Willis, R.M. Hoffman, C.G. Figdor, S.J. Weiss, and P. Friedl. 2013. Physical limits of cell migration: Control by ECM space and nuclear deformation and tuning by proteolysis and traction force. *J. Cell Biol.* 201:1069–1084. http://dx.doi.org/10.1083/jcb.201210152

Wu, J., I.A. Kent, N. Shekhar, T.J. Chancellor, A. Mendonca, R.B. Dickinson, and T.P. Lele. 2014. Actomyosin pulls to advance the nucleus in a migrating tissue cell. *Biophys. J.* 106:7–15. http://dx.doi.org/10.1016/j.bpj.2013.11.4489

Yu, X., T. Zech, L. McDonald, E.G. Gonzalez, A. Li, I. Macpherson, J.P. Schwarz, H. Spence, K. Futo, P. Timpson, et al. 2012. N-WASP coordinates the delivery and F-actin-mediated capture of MT1-MMP at invasive pseudopods. *J. Cell Biol.* 199:527–544. http://dx.doi.org/10.1083/jcb.201203025